Tunable FDM 3D printing of flexible poly(butylene adipate terephthalate)-based biocomposite filaments

Enhancing the On/Off Current Ratio in Single-Molecule FET via Destructive Quantum Interference

Chiara Elfi Spano, Yuri Ardesi, *Member, IEEE*, Gianluca Piccinini, and Mariagrazia Graziano

***Abstract*— We investigate through atomistic calculation the electronic structure and transport properties of 3-phenylethynylene (OPE3), 7-phenylvynylene (OPV7), and [3,3]paraCyclophane (pCp)-based molecules. We reveal and analyze the Destructive Quantum Interference (DQI) phenomenon for the pCp single-molecule junction. The provided explanation of DQI via the dominant concurrence of inter-orbital and intra-orbital interference may support DQI engineering through the chemical synthesis of *ad hoc* molecular channel. Furthermore, we propose a Back gate Biasing-based method for the ON/OFF CUrrent Ratio Enhancement of the single-molecule Field-Effect transistor via the control of DQI (BBB-CURE-DQI). As an important outcome of the proposed method, an ON/OFF current ratio of 10^3 is achieved for pCp single-molecule FET. This value is orders of magnitude larger than typical values presented in the literature. The benefit of the DQI and the effectiveness of the BBB-CURE-DQI method are finally demonstrated at the circuital level by SPICE simulations of digital inverters implemented with the investigated molecules. Our analysis and results motivate the importance of future research investment for DQI manipulation via chemical synthesis and successive control to enable single-molecule FET-based nanocomputing applications.**

***Index Terms*— Nanocomputing, paracyclophanes (pCps), quantum interference (QI), single-molecule transistor.**

I. Introduction

In THE last 50 years, Moore's law fed the progress of the computing field. Nowadays, fabrication costs and increasing demand for ultra-integrated, high-performing, low-power systems are becoming incredibly challenging, pushing the research toward Beyond-CMOS technologies. In this scenario, molecular devices are proved to be promising [1], [2], [3]. In particular, a substantial effort has been spent in the last two decades to experimentally demonstrate and model the single-molecule field-effect transistor (MolFET) [4], [5]. Because of the intrinsic nanometric molecule size (few Å), the MolFET may extend Moore's law to unforeseen limits, enabling an unparalleled level of integration at cheap manufacturing costs thanks to self-assembly techniques [6]. Furthermore, the electronic properties of molecular devices can be engineered by chemical synthesis with vast degrees of freedom. This controllability is a revolutionizing key with no parallel in solid-state technology at present [2]. Since the first evidence of the gating effect in a molecular junction [7], there has been in literature a proliferation of experimental works aiming at enhancing the MolFET fabrication process yield and performing reliable conductance measurements [8], [9]. Conventionally, the most common molecules used were the fully conjugated ones, e.g., benzene-dithiol (BDT), oligophenylethynylene (OPE), and oligophenylvynylene (OPV). They show impressive values of current for a single molecule (few μA) thanks to an optimal degree of π-conjugation that permits a good wave function delocalization throughout the molecule. However, because of high leakages, they are tough to be switched off, and thus, MolFETs based on these molecules exhibit a poor ON/OFF current ratio (I_{ON}/I_{OFF}).

In this work, we study through atomistic calculations the electronic structure and transport properties of two fully conjugated molecules (OPE3, OPV7) and [3,3]paraCyclophane (pCp)-based molecule. We reveal for the pCp a prominent Destructive Quantum Interference (DQI) effect, crucial in suppressing the current, thus for nanocomputing applications of the MolFET. By tracing back the DQI to intra-orbital and inter-orbital interference mechanisms, we provide helpful insights for DQI engineering (e.g., induction or intensification) via chemical synthesis. Then, we propose a Back-gate Biasing-based method for ON/OFF CUrrent Ratio Enhancement via DQI control (BBB-CURE-DQI) in MolFETs. We apply the BBB-CURE-DQI method to pCp-FET, and we validate the method effectiveness by achieving an I_{ON}/I_{OFF} one or two orders of magnitude larger than typical values presented in the literature for MolFET. Finally, a digital inverter realized with pCp-FETs is simulated and compared in terms of functioning with an OPV7-based implementation. This final circuital comparison justifies the crucial role of DQI and the necessity of its engineering and effective control for MolFET-based nanocomputing.

II. Background: The Single-Molecule Transistor

The MolFET is a three-terminal device in which the drain current I_{DS} is modulated by the gate voltage V_{GS}.

Manuscript received 23 June 2022; accepted 1 August 2022. Date of publication 18 August 2022; date of current version 22 September 2022. The review of this article was arranged by Editor B. Iñiguez. *(Corresponding author: Chiara Elfi Spano.)*

Chiara Elfi Spano, Yuri Ardesi, and Gianluca Piccinini are with the Department of Electronics and Telecommunications, Politecnico di Torino, 10129 Turin, Italy (e-mail: chiaraelfi.spano@polito.it).

Mariagrazia Graziano is with the Department of Applied Science and Technology, Politecnico di Torino, 10129 Turin, Italy.

Color versions of one or more figures in this article are available at https://doi.org/10.1109/TED.2022.3198025.

Digital Object Identifier 10.1109/TED.2022.3198025

The active channel is constituted by a single molecule chemically anchored to two nano-gaped electrodes through suitable linkers. The electrodes, acting as source (S) and drain (D), are typically made of gold (Au), and thiols (-SH) are commonly used as linkers since they provide strong covalent bonds with Au. The channel is electrostatically coupled to a third gate electrode. The MolFET is thus modeled as a quantum dot coupled to S and D contacts. Molecular energy levels characterize the quantum dot, whereas the S/D Fermi level $\mu_{S/D}$ the S and D electrodes. At equilibrium, $\mu_{S/D}$ are aligned with the Fermi level of the molecular dot, while out-of-equilibrium, I_{DS} is generally expressed as [5]

$$I_{\mathrm{DS}} = \frac{2q}{h}\int_{-\infty}^{+\infty} T(E)[f_S(E,\mu_S) - f_D(E,\mu_D)]dE \quad (1)$$

where q is the electron charge, h the Planck's constant, E is the electron energy, $f_{S/D}$ are S/D Fermi's distributions, and $T(E)$ the transmission spectrum representing the transmittivity of the molecular channel. In the coherent tunneling limit, (1) reduces to the Landauer–Büttiker formula, where $T(E)$ is defined within the Non-Equilibrium Green's Function (NEGF) formalism as [10]: $T(E) \equiv \mathrm{Tr}[G^R(E)\Gamma_S(E)G^A(E)\Gamma_D(E)]$, with Tr the trace operator, $G^{R/A}$ the retarded/advanced Green's functions, and $\Gamma_{S/D}$ the S/D broadening functions. The latter two represent the contacts-molecule coupling strength and quantify the broadening effect of the contact electrodes on the energy levels of the molecular dot. Furthermore, $\Gamma_{S/D}$ are related to the intrinsic time τ through the relation: $\Gamma = h/\tau$, where Γ corresponds to the total broadening function ($\Gamma = \Gamma_S + \Gamma_D$). The intrinsic time measures the time required for a transmitting electron to pass from one contact to the other. The Landuer–Büttiker formula assumes that during τ, the electron preserves its phase coherence and does not undergo inelastic scattering. There is evidence that this assumption is reasonable, especially for short enough molecules having large values of Γ, i.e., chemisorbed to the electrodes via suitable linkers assuring strong covalent bonds [11], [12]. However, for long and weakly coupled molecules (above few nm), τ increases. This increase means that decoherence and vibrational-induced decoherence effects (due to molecular vibrations) may become non-negligible for an electron traveling through the molecule and thus, must be included in a more general definition of $T(E)$ [13]: $T(E) \equiv \mathrm{Tr}[\Sigma^{<}G^{>}(E) - \Sigma^{>}G^{<}(E)]$. This more general definition of $T(E)$, where $\Sigma^{\lessgtr}$ are the lesser/greater contact self-energies and $G^{\lessgtr}$ are the lesser/greater Green's functions, turns (1) into the Meir–Wingreen formula. The lesser/greater contact self-energies $\Sigma^{\lessgtr}$ represent the overall effect of the contact electrodes on the molecular channel in the shifting and broadening of the energy levels corresponding to Γ. The lesser/greater Green's functions $G^{\lessgtr}$ are related to the above-mentioned retarded and advanced Green's functions (i.e., non-interacting ones) and the total self-energy Σ_{tot} via the Keldysh equation: $G^{\lessgtr} = G^R\Sigma_{\mathrm{tot}}^{\lessgtr}G^A$. The total self-energy Σ_{tot} is the sum of all the relevant self-energies in the system under investigation (contacts, interactions). It includes Σ_{ph}, the self-energy that models the interaction effects between transmitting electrons and molecular vibrations (i.e., electron–phonons (e-ph) interactions).

In summary, τ represents a fundamental timescale parameter that discriminates between two transport regimes: the purely coherent elastic well described by Landauer–Büttiker formula, and the incoherent one modeled with the more general Meir–Wingreen formula.

In general, from (1), it is evident that the molecular energy levels that contribute to conduction are those within μ_S and μ_D. This strictly holds at 0 K, whereas at room temperature, the thermal spreading is considered with the tails of the Fermi distributions. We refer to the energy spacing between μ_S and μ_D induced by D-to-S voltage V_{DS} as bias window (BW). The application of V_{GS} allows the modulation of I_{DS} by shifting the molecular energy levels falling within the BW [5] and by properly tuning a back gate voltage (by the use of an additional gate electrode), conduction of n- or p-type can be selected. The former is mediated through the Lowest Unoccupied Molecular Orbital (LUMO), while the latter through the Highest Occupied Molecular Orbital (HOMO). Moreover, by the back gate bias tuning, an enhancement of $I_{\mathrm{ON}}/I_{\mathrm{OFF}}$ can also be achieved as proved in Section IV. Furthermore, beyond the Landauer–Büttiker limit, additional transmitting channels due to phonons adsorption/emission may be included in the BW, thus contributing to the increase of $T(E)$ and consequently of I_{DS} [14].

Besides the interactions, $T(E)$ is influenced by a variety of factors [15], [16]: the type of molecule and its conformation (constituting chemical elements, bond angles, and lengths), the molecular length, the type of linkers, and the materials and geometries of the electrodes. The latter determines the molecule-contact coupling strength ($\Gamma_{S/D}$) and thus strongly affects the broadening of the peaks of $T(E)$. Moreover, the gate-stack materials and geometry define the molecular channel's electrostatic control, thus the gate potential's effectiveness in I_{DS} modulation. This wide degree of freedom in manipulating the MolFET conduction is a crucial feature with no parallel in solid-state devices. Recently, the discovery of Quantum Interference (QI) in molecular junctions [17], [18] has introduced another degree of freedom in MolFET engineering. QI occurs thanks to the interference of the Molecular Orbitals (MOs) contributing to a specific transmission state. If the MOs-i.e., the 3-D space projection of the electron wavefunctions-involved are in-phase, they constructively interfere, giving rise to resonance peaks with high transmittivity in $T(E)$, while if out-of-phase, they destructively interfere, leading to anti-resonance peaks in $T(E)$. The fingerprint of DQI is an abrupt dip in the transmittivity for a small energy range near E_F. Exploiting or even manipulating the QI by chemical synthesis may be the long-sought key to enable high-performance MolFETs.

Note that for short molecules strongly coupled with the contacts, decoherence, or vibrationally induced decoherence effects represent weak perturbations. Therefore, the DQI phenomenon-if present-is almost unaffected and may be accurately described within the Landauer–Büttiker realm. Differently, for longer molecules or vibrationally highly excited and weakly coupled molecules (small Γ), decoherence effects and vibronic coupling might lead to the quenching of the DQI phenomenon-if present. Thus, in this latter case, by describing

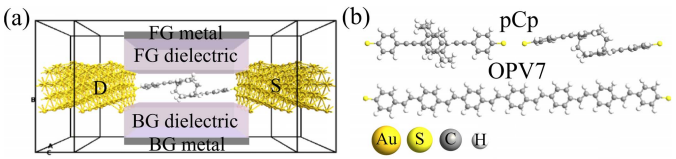

Fig. 1. (a) Device configuration of the pCp-FET. (b) Front and top views of the isolated pCp and the front view of the isolated OPV7.

the DQI phenomenon within a purely coherent elastic picture, quantitatively inaccurate results may be obtained.

III. Computational Methodology

We study and compare the electronic structure and transport properties of OPE3, OPV7, and pCp molecules firstly in their isolated and single-molecule junction configuration (see Section IV-A). This analysis provides guidelines for the engineering step of their ambipolar MolFET configuration. Fig. 1(a) shows the structure of the simulated MolFETs. They are constituted by atomistic Au FCC (111) S and D electrodes and Front (FG) and Back (BG) metal Gates. We choose a double-gate configuration with a single atomic layer of ZrO_2 (thickness 5.7 Å) as gate dielectric to get effective electrostatic control of the channel. Indeed, ZrO_2 provides a better equivalent oxide thickness if compared to the common HfO_2 thanks to its higher dielectric constant.

The BG voltage values V_{BG} are carefully chosen according to the BBB-CURE-DQI method proposed in Section IV-B. After this engineering step, the two MolFETs are characterized through atomistic simulations. All the electronic structure calculation are performed self-consistently in QuantumATK (v. Q-2019.12) [19] employing Extended Hückel theory (EHT) coupled with the NEGF method for transport properties calculation. Dirichlet Boundary Conditions (BCs) are used in the transport direction, while Neumann BCs along the metal gate stacks and periodic BCs elsewhere. For both MolFETs, covalent Au-S bonds assure strong contacts-molecule coupling. Thus, the transport mechanism, especially for the shorter pCp molecule, is assumed to be mainly coherent tunneling, and the transport calculation are performed within the Landauer–Büttiker limit at 300 K. This assumption permits obtaining results at a sustained computational cost. To evaluate the validity of this assumption and thus the accuracy of the obtained results, we also evaluate at 300 K the inelastic effects by taking into account e-ph interactions in the dynamical region of the device-i.e., molecular channel, including the linkers. We restrict this validation only to the MolFET engineered via DQI control (pCp-FET). The e-ph coupling self-energies Σ_{ph} are computed within the self-consistent Born approximation (SCBA) by first evaluating the phonon modes (i.e., the dynamical matrix) and then the e-ph coupling matrix for each phonon mode. The inelastic $T(E)$ is finally computed with the extended lowest order expansion (XLOE) method [13] and the inelastic contribution to the total current is derived. Current–voltage characteristics simulated within the coherent tunneling limit, are stored in a Lookup table (LUT), and by employing the LUT-based model presented in our previous work [20], we perform the functional verification of MolFET-based digital inverters (see Section IV-C) in Cadence Virtuoso.

IV. Simulation Results and Discussion

A. Isolated Molecule and Single-Molecule Junction

Fig. 1(b) shows the front and top view of a phenyl-ethynyl-dithiol-based wire connected to a [3.3]pCp-core and a phenyl-vynylen-dithiol wire made of seven phenyl rings. We referred to the former as pCp and to the latter as OPV7. The pCp core is made of two faced-benzene rings bridged through three methylene groups. This peculiar conformation breaks the planarity and thus the conjugation of the system, leading to unique electronic properties and inter-ring interactions. Contrarily to pCp, OPV7 is a planar aromatic molecule. Consequently, it is a fully conjugated molecule since there is no break in the π-conjugation due, e.g., to inter-ring torsion.

From electronic structure simulations, the isolated pCp molecule has 164 electrons. According to the Pauli exclusion principle, each energy state-i.e., MOs-can have an occupancy equal to two electrons with different spins; thus, MO with quantum number 81 corresponds to the HOMO, while 82 to the LUMO. The OPV7 has 258 electrons; thus, MO 128 is the HOMO and 129 the LUMO. Both molecules exhibit a small HOMO-LUMO Gap (HLG), like most of the molecules belonging to the aromatic class: 2.81 eV for pCp, and 1.05 eV for OPV7. Furthermore, long molecules like OPV7 (47 Å in length) typically mean a larger number of atoms constituting the molecule itself. More atoms lead to a greater number of bonding and anti-bonding energy states, thus reducing HLG and explaining the smaller value for OPV7 with respect to the HLG of pCp (20.7 Å in length).

In Fig. 2(a), the allowed main energy states of the isolated molecules are superimposed on the Density of States (DOS) projected on the molecular channel (i.e., projected DOS). As expected from theoretical and experimental findings [5], the discrete energy levels of the isolated molecules are shifted down in energy and broadened when the molecules anchor to the Au electrodes, i.e., when the molecular junction is created. This effect is due to the molecule–electrode surface interaction. In particular, the amount of the broadening depends on the coupling strength Γ of the electrodes-acting as bulky reservoirs of electron states-on the molecular channel. It is determined mainly by the material type and geometrical orientation of the electrodes with respect to the molecular channel, the suitability of the anchoring groups in creating strong covalent bonds with the electrodes, and the molecular length. Since the two device configurations differ only on the molecular channel, the length of the molecule is the main reason for the difference between the DOS. Indeed, shorter molecules exhibit larger coupling factors, explaining the broader resonance peaks of the DOS for pCp. Furthermore, the DOS analysis results in the dominant contribution of p orbitals for both molecules, which favor creating π-bonds throughout the molecules. The presence of π-bonds leads in turn to a great delocalization of the electron wave function (Ψ), which means that electrons are not strictly bounded but shared between single atoms composing the molecule and thus free to move if a perturbation is applied. Small HLG and Ψ delocalization imply the suitability for conduction for both the considered molecules if compared to, e.g., alkanes, which

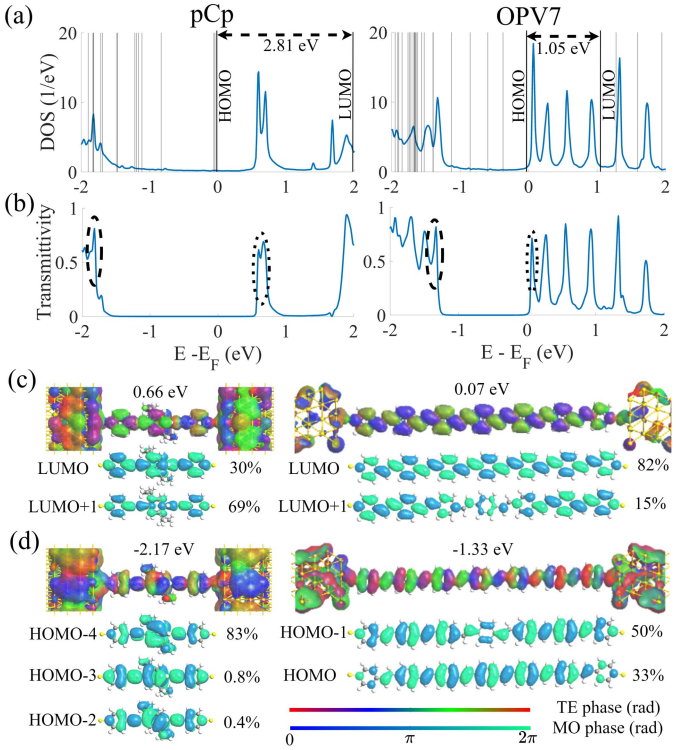

Fig. 2. (a) Computed discrete energy states of the isolated molecules superimposed in energy to the projected DOS for pCp and OPV7. The HOMO and LUMO are labeled and the HLGs are marked with double arrows. (b) Computed $T(E)$ for pCp and OPV7 FETs at equilibrium. The Main TEs and the corresponding dominant MOs for the transmission peaks (c) above and (d) below E_F, for pCp and OPV7 FETs. The isosurface values are 0.1 for TE and 0.01 for MO.

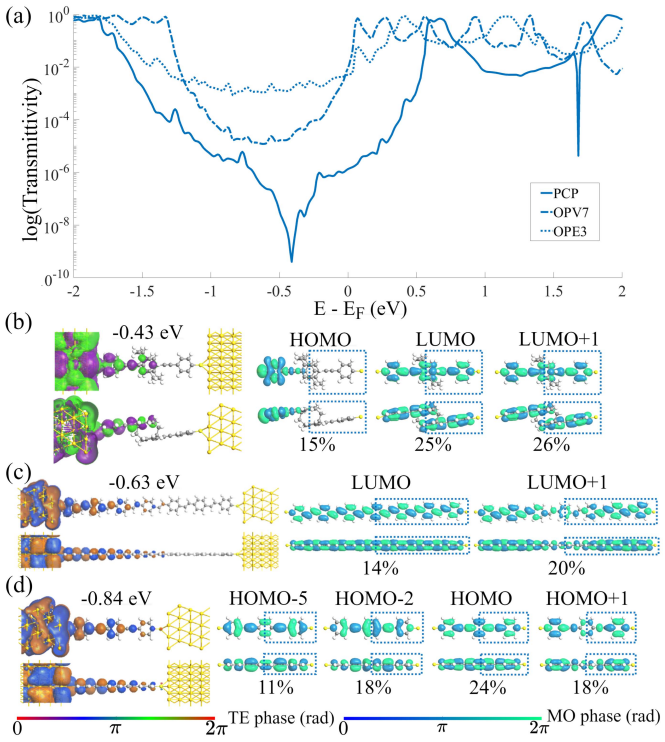

Fig. 3. (a) Equilibrium $T(E)$ in semi-logarithmic scale for pCp, OPV7, and OPE3 FETs. The main TEs and the corresponding MOs at the lowest anti-resonance values for (b) PCP, (c) OPV7, and (d) OPE3 FETs. The isosurface values are 0.1 for TE and 0.01 for MO.

behave like molecular insulators (HLG$\simeq 7 \div 9$ eV and σ-bonds dominance). This suitability is also confirmed in Fig. 2(b) by the high transmittivity $T(E)$ for the two devices. Note that in both cases, the $T(E)$ peaks resemble the corresponding peaks in the DOS.

Regarding the main $T(E)$ peaks, the following important considerations hold. Considering the peaks above E_F for both devices (dotted ellipsis), it is evident that the transmission peak of the OPV7 device centered at 0.07 eV is narrower with respect to the pCp one centered at 0.66 eV. This difference is due to a stronger electrode coupling for the pCp device. This causality is confirmed by the corresponding Transmission Eigenstates (TEs) that mainly contribute to the two considered transmission peaks. They are solutions of the quantum mechanical eigenproblem for the transmission operator projected in the space domain, i.e., surfaces of iso-transmission probability for a specific energy value. The amplitude of the surfaces denotes the magnitude of transmission probability, while the color represents the phase of the transmitted electrons. The TE of OPV7 shows a vanishing surface on the sulfur linkers-atoms located at the chain ends-and, thus, a smaller overlap with the Au states with respect to the pCp case. These small electrode-linker states overlap of the OPV7 TE is the cause of a weaker coupling, thus of the localized peak in the DOS and consequently of the sharp transmission peak considered. Similar considerations hold for the resonance peaks below E_F for pCp and OPV7 (dashed ellipsis). They are both narrow peaks but very close to other narrow peaks. This proximity forms a broadened resonance band overall, explaining the large overlap of Sulfur and Au states in the corresponding TEs of Fig. 2(d). This large overlap reveals a good electrode coupling for both devices at that specific energy range.

Fig. 2(c) and (d), show the MOs with a larger contribution to the corresponding TE, i.e., the MOs that are mainly responsible for the transmission. In particular, the transmittivity of the largest TE above E_F for both molecules is mainly due to the superposition of LUMO and LUMO + 1 with the reported percentages. Note in both cases the consistency in shape and phases of the TE with the dominant MO. This consistency also occurs for the resonance peaks below E_F. For pCp, the TE has a dominant singular state contribution from HOMO-4, whereas, for OPV7, the transmission is carried by the superposition of HOMO-1 and HOMO with the reported percentage. Fig. 3(a) shows the equilibrium $T(E)$ in logarithmic scale for pCp and two fully-conjugated molecules typically investigated in Molecular Electronics literature, namely OPV7 and OPE3. The $T(E)$ trend shows the peculiarity of the pCp molecule with respect to the other conventional ones: the abrupt dip in-depth in the transmittivity for a small energy range near the E_F is a clear fingerprint of DQI. This peculiarity is not shown by the other two molecules, where the anti-resonance region is much more gradual and smooth without an actual dip in-depth to a shallow value of transmittivity. In particular, the transmittivity of pCp molecule at -0.43 eV reaches values of 10^{-9}, four and seven orders of magnitude less with respect to the OPV7 and OPE3 cases, respectively. These differences in transmittivity values can be traced back to the corresponding TEs, and MOs reported in Fig. 3(b)–(d). In particular, in Fig. 3(b) are reported the largest TEs and

the main MOs contributing to the DQI for pCp, while in Fig. 3(c) and (d), the ones contributing to the lowest anti-resonance peaks for OPV7 and OPE3, respectively. In each case, the TE clearly shows a transmission bottleneck, i.e., a vanishing iso-transmission surface along the molecule toward the S electrode. This transmission bottleneck is prominent in the last three phenyl rings of OPV7 and the last phenyl ring of the pCp molecule, while it is less emphasized in OPE3. This trend reflects the transmittivity of the three devices in the aforementioned orders of magnitude. On the right side of Fig. 3(b)–(d), the MOs giving rise to the transmission bottleneck are reported with their contribution percentage. These results confirm that, actually, the DQI occurs for all three devices, but more prominently for pCp. Indeed, by inspecting the MOs for each case, it is evident there is a portion along the molecules (blue rectangles) in which the MOs have opposite phases and thus interfere destructively one each other. However, the actual difference that makes the DQI in the pCp molecule so prominent is that LUMO and LUMO + 1 in that highlighted region interfere with almost the same weight in magnitude (25% and 26%), thus canceling the transmittivity for that specific energy value. Furthermore, the deep anti-resonance peak in the transmittivity of pCp is determined by interfering MOs-also known as "inter-orbital" DQI-, but also heavily by the contribution of a single MO, the HOMO, that is itself a result of DQI. This latter type of DQI, named "intra-orbital" DQI, is a result of destructive interference of atomic orbitals combining to obtain MOs when solving the Shrödinger equation [21]. The delocalization and magnitude of the TE resemble, in that region, the negligible electron probability of the HOMO, thus confirming its strong influence.

B. Single-Molecule FET and BBB-CURE-DQI Method

Fig. 4 reports the evolution of the $T(E)$ as a function of voltage perturbations for pCp device. In particular, Fig. 4(a) shows the effect of the V_{DS} only. The resulting $T(E)$ evolution is almost mirrored for positive and negative values of V_{DS} thanks to the molecule's symmetry. Thus, reversing the bias polarity does not lead to a noticeable difference in the transport properties. Considering the portion of the $T(E)$ for positive values of V_{DS}, it is evident that the location in the energy of the peaks remains quite unchanged for V_{DS} lower than 0.9 V. However, by increasing V_{DS} the BW (dotted white lines) enlarges, including more energy states. The newly involved states get occupied by incoming electrons from electrodes and become transmission states. This results in a greater current. However, the occupancy of before empty energy states leads to an increase in the molecule's potential energy (also known as charging effect), thus to an upward shift of the energy states themselves and the corresponding $T(E)$ peaks. Therefore, the bias-induced entry of new energy states leads in turn to a getaway of themselves, which become now accessible for larger BWs. This getaway hampers the conduction and reduces the current with an increasing bias voltage V_{DS}, i.e., in a Negative Differential Resistance (NDR) trend. Therefore, e.g., the transmission peak around 0.5 eV at equilibrium, once it is close to being included in the BW, it is pushed upward in energy.

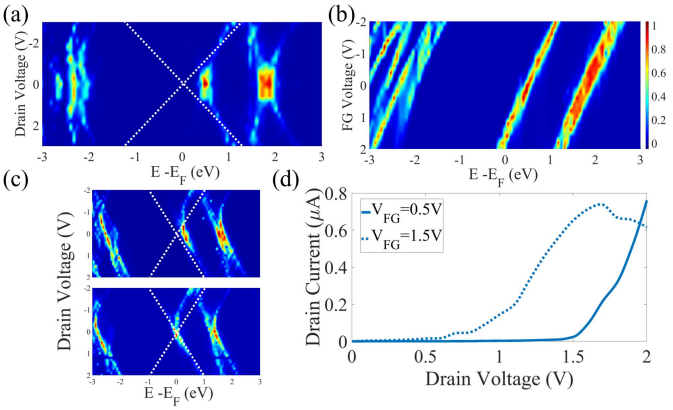

Fig. 4. (a) Effect of V_{DS} on $T(E)$, at $V_{BG} = V_{FG} = 0$ V. (b) Gating effect on $T(E)$, with $V_{FG} = V_{DS} = 0$ V. (c) Superposition of V_{DS} and gating effect on $T(E)$. In particular, the $T(E)$ evolution depending on V_{DS} at $V_{FG} = 0.5$ V (top) and $V_{FG} = 1.5$ V (bottom), for $V_{FG} = 0$ V. (d) Computed output characteristic $I_{DS}(V_{DS})$ for $V_{FG} = 0.5$ V (blue) and $V_{FG} = 1.5$ V (dotted blue) $V_{FG} = 0$ V. All plots refer to pCp-FET. The BW is represented with dotted white lines.

Fig. 4(b) clearly demonstrates the gating effect. It is obtained by varying V_{FG} from negative to positive values for a null BW, and it consists of an almost rigid translation of the $T(E)$ toward, respectively, greater or lower energies. The amount of translation depends on the electrostatic strength of the considered gate terminal, identified by the so-called coupling gate factor (α). It is defined as the ratio between the variation in energy (ΔE) and the potential applied to achieve that variation ($\Delta q V_{DS}$), in formulae: $\alpha = (\Delta E / \Delta q V_{DS})$. In particular, the FG's specific material properties and spatial arrangement provide $\alpha_{FG} = 0.58$, while for BG $\alpha_{BG} = 0.53$. Indeed, a lower amount of $T(E)$ translation due to the application of BG voltage results from simulations. Fig. 4(c) shows the superposition of both V_{DS} and FG voltage V_{FG} effects for $V_{FG} = 0.5$ and 1.5 V, while Fig. 4(d) reports the resulting output characteristic $I_{DS}(V_{DS})$. In both cases, it is evident the gating and charging effect. The former is responsible for the overall rigid translation toward lower energies of the $T(E)$ evolution thanks to an increasing positive V_{FG}. This shift is larger for 1.5 V of V_{FG}, and therefore the main transmission peaks above E_F are included before in the BW, thus contributing to the current for lower V_{DS} as demonstrated in the output characteristic. Instead, the latter is evident in the $T(E)$ upward getaway with increasing BW. This getaway is especially steep in the case $V_{FG} = 1.5$ V, and consequently, this results in an NDR trend in the output characteristic for V_{DS} values above 1.6 V.

Fig. 5(a) and (b), reports, respectively, the output and trans characteristics of the ambipolar pCp-FET optimized through the BBB-CURE-DQI method. It consists of the following.

1) By inspecting the equilibrium $T(E)$ (e.g., the one of Fig. 3), identifying a proper range of V_{FG} for which simulate the n and p device configurations at fixed $V_{FG,ON}$ and $V_{FG,OFF}$. Indeed, aware of the gating and charging effect and once α_{BG} is known, it is enough to inspect the equilibrium $T(E)$ to choose the proper V_{FG} sweep range that allows simulating the device when the resonance peaks of LUMO and HOMO types and the DQI anti-resonance peaks are included in the BW. By including the HOMO peak in the BW, the p-type

is simulated, while by including the LUMO ones, the n-type. In both cases, they are simulated at the ON state, whereas also including the DQI anti-resonance peaks, they are both simulated in their OFF state.

2) From the analysis of simulation results of step 1), choose the exact V_{FG} value for n and p MolFETs so that the following device-level specifications are satisfied.
   a) Ambipolar feature (i.e., p- and n-MolFET with symmetric threshold voltages: $|\ V_{THn}\ | = |\ V_{THp}\ |$) suitable for static CMOS logic circuits.
   b) Satisfying values of ON current (I_{ON}) to get an adequate driving strength.
   c) I_{ON}/I_{OFF} as much as possible close to the minimum requirement for modern digital circuits (10^4) with I_{OFF} as low as possible to minimize static power consumption due to leakages. This requirement is achieved by choosing a V_{FG} value that allows the DQI dip in the $T(E)$ to be included within the BW when the FG voltage that switches OFF the MolFET ($V_{FG,OFF}$) is applied.
   d) An I_{ON} for the n-type similar to the one for p-type ($|\ I_{ONn}\ | \simeq |\ I_{ONp}\ |$) to minimize circuit noise margins and delays.

Notice that the BBB-CURE method is also applicable for molecules not exhibiting DQI dip in the transmittivity, like OPV7 or OPE3. Indeed, it is enough to choose a V_{FG} value that allows the lowest anti-resonance peak in the $T(E)$ to be included within the BW when $V_{FG,OFF}$ is applied, and include the HOMO/LUMO peak when $V_{FG,ON_{p/n}}$ is applied.

We apply to pCp-FET the BBB-CURE-DQI method. The chosen V_{FG} sweep range results $[-4, 2]$ V, and the optimum values of V_{FG} for pCp n- and p- FETs results 1.2 and -3.3 V. After this optimization step, the pCp ambipolar MolFET is characterized. The output and trans characteristics in Fig. 5(a) and (b) are plotted, respectively, for the optimal V_{FG} values. In particular, the output characteristics are plotted for V_{FG} values for which the MolFETs turn ON ($V_{FG,ON}$, continuous lines) or OFF ($V_{FG,OFF}$, dotted lines). The trends are similar to the ones of conventional FET (parabolic for low values of V_{DS}, almost linear, and then a saturation region), besides the little NDR trend that occurs for p-MolFET. The computed I_{ON} (continuous line curves), that is the I_{DS} for $V_{FG,ON}$ at $V_{DS} = 1$ V for n-type and $V_{DS} = -1$ V for p-type, are pretty large values for a single molecule. Consequently, this will not affect too much the propagation delay of the MolFET-based digital circuit. Moreover, considering the same molecule, the I_{ON} are quite similar in magnitude for n and p types; this ensures almost the same driving strengths for pull-up and pull-down transistors in a static CMOS logic cell, thus minimizing noise margins and delays. It results 0.27 and -0.34 μA, respectively, for n and p-type pCp-FET. The computed I_{OFF} (dotted line curves), that is the I_{DS} for $V_{FG,OFF}$ at $V_{DS} = 1$ V for n-type and $V_{DS} = -1$ V for p-type is of the order of pA for pCp-FETs (n: 0.18 nA; p: -0.23 nA). The pCp-FETs are thus effectively turned OFF and the resulting I_{ON}/I_{OFF} is surprisingly high for a single-molecule (1452 for n-type and 1478 for p-type). We apply the BBB-CURE method for OPV7-FET obtaining a quite large I_{OFF} (n: 24.32 nA; p: -28.56 nA) and an I_{ON}/I_{OFF} of 42 for n-type and 54 for p-type. The two orders of magnitude of difference in the I_{ON}/I_{OFF} between the two MolFETs demonstrate the importance of the presence of the DQI phenomenon for MolFET and the effectiveness of the proposed BBB-CURE-DQI method in DQI control to optimize them.

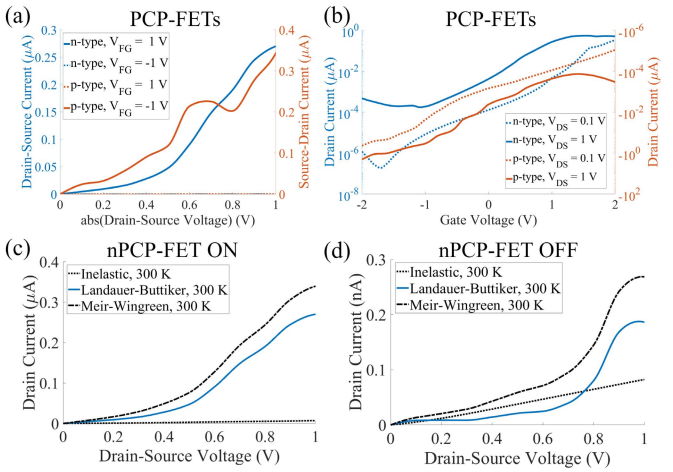

Fig. 5. (a) Output characteristics of the n and p-type pCp-FET at $V_{FG,ON}$ (continuous lines) and $V_{FG,OFF}$ (dotted lines). (b) Transcharacteristics at low (dotted blue and red lines) and high V_{DS} (continuous lines); output characteristics of n-type pCp-FET in (c) ON and (d) OFF states. The dotted black curves are the currents resulting from inelastic effects, the blue ones are the currents calculated within the Landauer–Büttiker limit (elastic), whereas the dashed black are the currents calculated with Meir–Wingreen formula (inelastic + elastic). For (a)–(d), $V_{FG} = 1.2$ and -3.3 V are fixed for n- and p-type, respectively.

Fig. 5(c) and (d) report the output characteristics of the n-type pCp-FET at $V_{FG,ON}$ and $V_{FG,OFF}$, respectively. The blue curves correspond to the currents calculated within the Landauer–Büttiker limit whereas the dashed black ones correspond to the currents calculated through the more general and accurate Meir–Wingreen formula. Therefore, the former blue curves include only coherent and elastic contributions, and the latter black ones also the inelastic ones. The dotted black lines are the currents derived only by the inelastic effects due to transmitting electrons interacting with all 185 molecular vibration modes of pCp molecule. The inclusion of the inelastic contribution, which provides more realistic results, leads to imperceptible increases in the ON current (+6.9 nA) and a more appreciable but still slight increase in the OFF current (+0.082 nA). Therefore, the considered inelastic contributions lead to a small suppression of the DQI phenomenon also at room temperature, and as a consequence, the resulting impact on the ON/OFF current ratio of the n-type pCp-FET is non-negligible (reduction of 28.8% at 300 K) but still contained. Indeed, the n-type pCp-FET still has a substantial I_{ON}/I_{OFF} of 10^3 (1032 at 300 K), thus the above considerations and outcomes still holds. Similar results and percentage of ON/OFF current ratio reduction are expected for the p-type whose transmission is mediated via electrons having the same order of magnitude of energy.

C. Single-Molecule FET-Based Digital Inverter

The optimized pCp and OPV7 FET-based inverters are finally designed in Cadence Virtuoso. Fig. 6(a) shows the schematic of the molecular circuit and Fig. 6(b) the results of the functional verification we perform for the OPV7 (dotted

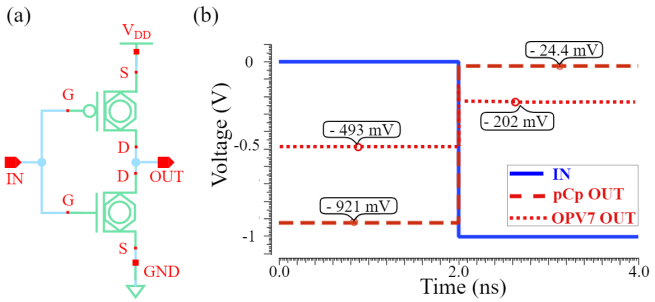

Fig. 6. (a) Schematic of the MolFET-based inverter. (b) Simulation results of the pCp- and OPV7- based inverter functional verification. The blue line is the input signal (IN), while the red lines are the output signal of the pCp (dashed) and OPV7 (dotted).

lines) and pCp (dashed lines) FET-based inverters. Note that the values obtained are steady-state values since the LUT collects the static physical simulation results. Transient quantities are not present; thus, delays of the logic gates are not measurable and are out of the scope of this circuital section, whose principal aim is to verify the correct functioning of the inverters and relate it to the DQI phenomena.

From the functional verification, it is evident how the presence of DQI and application of the BBB-CURE-DQI method are essential in obtaining an inverter performing the NOT function or, more in general, in obtaining logic gates correctly working. Indeed, thanks to an acceptable I_{ON}/I_{OFF}, when a logic "1"—encoded in 0 V—is asserted at the input, the npCp-FET is able to pull down the output line toward the ground (corresponding to -1 V) because the p-type is more effectively turned OFF with respect to the OPV7 case. As a result, a logic "0"—encoded in -1 V—is obtained at the output of the pCp-FET based inverter with an acceptable reduction of the noise margins (3% for "1" and 8% for "0"). Whereas for the OPV7 case, the leakage is too high that the pMolFET continues to conduct, making it more difficult for the n-type to pull down the output line. Thus, the logic gate is not correctly inverting the input signal. Analogous consideration for logic "0" case in input.

V. Conclusion

We perform a comprehensive simulation-based electronic structure and transport properties study to reveal and explain the DQI phenomenon in pCp molecular junction. The proposed BBB-CURE-DQI method, which manipulates QI to switch between conductive CQI and insulative DQI molecular transmission states, allows the engineering of ambipolar double-gate MolFETs for digital circuit applications. As an important outcome of the adopted method, an I_{ON}/I_{OFF} of 10^3 is obtained for pCp-FETs. This value is orders of magnitude larger than typical values presented in the literature. Furthermore, by comparing the optimized pCp-FET and OPV7-FET, we demonstrate the benefits of the DQI and BBB-CURE-DQI method at the circuital level in terms of functioning. Indeed, the inverter based on pCp-FETs is able to correctly invert the input signal, contrarly to OPV7-FETs based one, because of too high reduction of noise margins. This circuital level final comparison justifies the crucial role of DQI and the necessity of its engineering and effective control to enable high-performance MolFET for nanocomputing applications.

References

[1] M. Ratner, "A brief history of molecular electronics," *Nature Nanotechnol.*, vol. 8, no. 6, pp. 378–381, Jun. 2013.
[2] D. Xiang, X. Wang, C. Jia, T. Lee, and X. Guo, "Molecular-scale electronics: From concept to function," *Chem. Rev.*, vol. 116, no. 7, pp. 4318–4440, Apr. 2016.
[3] Y. Ardesi, A. Pulimeno, M. Graziano, F. Riente, and G. Piccinini, "Effectiveness of molecules for quantum cellular automata as computing devices," *J. Low Power Electron. Appl.*, vol. 8, no. 3, p. 24, Jul. 2018, doi: 10.3390/jlpea8030024.
[4] H. Song, Y. Kim, Y. H. Jang, H. Jeong, M. A. Reed, and T. Lee, "Observation of molecular orbital gating," *Nature*, vol. 462, no. 7276, pp. 1039–1043, Dec. 2009, doi: 10.1038/nature08639.
[5] S. Datta, *Quantum Transport: Atom to Transistor*. Cambridge, U.K.: Cambridge Univ. Press, 2005, doi: 10.1017/CBO9781139164313.
[6] G. M. Whitesides and M. Boncheva, "Beyond molecules: Self-assembly of mesoscopic and macroscopic components," *Proc. Nat. Acad. Sci. USA*, vol. 99, no. 8, pp. 4769–4774, 2002.
[7] H. Park, J. Park, A. K. L. Lim, E. H. Anderson, A. P. Alivisatos, and P. L. McEuen, "Nanomechanical oscillations in a single-C_{60} transistor," *Nature*, vol. 407, no. 6800, pp. 57–60, Sep. 2000, doi: 10.1038/35024031.
[8] M. L. Perrin, E. Burzurí, and H. S. J. van der Zant, "Single-molecule transistors," *Chem. Soc. Rev.*, vol. 44, no. 4, pp. 902–919, 2015.
[9] V. Dubois *et al.*, "Massively parallel fabrication of crack-defined gold break junctions featuring sub-3 nm gaps for molecular devices," *Nature Commun.*, vol. 9, no. 1, p. 3433, Aug. 2018.
[10] S. Datta, "Nanoscale device modeling: The Green's function method," *Superlattices Microstruct.*, vol. 28, no. 4, pp. 253–278, Oct. 2000.
[11] C. J. Lambert, *Quantum Transport in Nanostructures and Molecules*. Bristol, U.K.: IOP Publishing, 2021, pp. 2053–2563.
[12] A. Danilov *et al.*, "Electronic transport in single molecule junctions: Control of the molecule-electrode coupling through intramolecular tunneling barriers," *Nano Lett.*, vol. 8, no. 1, pp. 1–5, 2008.
[13] T. Frederiksen, M. Paulsson, M. Brandbyge, and A.-P. Jauho, "Inelastic transport theory from first principles: Methodology and application to nanoscale devices," *Phys. Rev. B, Condens. Matter*, vol. 75, no. 20, May 2007, Art. no. 205413.
[14] M. A. Reed, "Inelastic electron tunneling spectroscopy," *Mater. Today*, vol. 11, no. 11, pp. 46–50, Nov. 2008.
[15] M. H. Garner, W. Bro-Jørgensen, P. D. Pedersen, and G. C. Solomon, "Reverse bond-length alternation in cumulenes: Candidates for increasing electronic transmission with length," *J. Phys. Chem. C*, vol. 122, no. 47, pp. 26777–26789, Nov. 2018.
[16] X.-X. Fu, R.-Q. Zhang, G.-P. Zhang, and Z.-L. Li, "Rectifying properties of oligo(phenylene ethynylene) heterometallic molecular junctions: Molecular length and side group effects," *Sci. Rep.*, vol. 4, no. 1, p. 6357, May 2015.
[17] H. Vazquez *et al.*, "Probing the conductance superposition law in single-molecule circuits with parallel paths," *Nature Nanotechnol.*, vol. 7, no. 10, pp. 663–667, Oct. 2012.
[18] C. R. Arroyo, R. Eelkema, F. C. Grozema, and H. S. J. van der Zant, "Signatures of quantum interference effects on charge transport through a single benzene ring," *Angew. Chem. Int. Ed.*, vol. 52, no. 11, pp. 3152–3155, 2013.
[19] S. Smidstrup *et al.*, "QuantumATK: An integrated platform of electronic and atomic-scale modelling tools," *J. Phys., Condens. Matter*, vol. 32, no. 1, Jan. 2020, Art. no. 015901.
[20] F. Mo, C. E. Spano, Y. Ardesi, G. Piccinini, and M. Graziano, "Beyond-CMOS artificial neuron: A simulation-based exploration of the molecular-FET," *IEEE Trans. Nanotechnol.*, vol. 20, pp. 903–911, 2021.
[21] C. J. Lambert and S.-X. Liu, "A magic ratio rule for beginners: A Chemist's guide to quantum interference in molecules," *Chem.-A Eur. J.*, vol. 24, no. 17, pp. 4193–4201, Mar. 2018, doi: 10.1002/chem.201704488.

Open Access funding provided by 'Politecnico di Torino' within the CRUI CARE Agreement